

EXPERIMENTS ON REDUCED SCALE FWT

Contents

5.1	Introduction	127
5.2	Experimental set-up	128
5.2.1	Real-time hybrid method	128
5.2.2	Reduced scale system	130
5.2.3	Numerical model	131
5.3	Controller design	131
5.3.1	GSPI control	132
5.3.2	LQR control	133
5.3.3	SAST control	134
5.4	Experimental results and analysis	135
5.4.1	Scenario 1. Step wind and still water conditions	136
5.4.2	Scenario 2. Stochastic wind and irregular wave condition	136
5.5	Conclusions	144

5.1 Introduction

In the previous chapters, high order sliding mode control with gain adaptation algorithms has been applied to floating wind turbine systems. Different control strategies, such as collective blade pitch control, individual blade pitch control and control combined with electric machine have been designed, all of those controllers being evaluated thanks to the co-simulations made by SIMULINK and FAST. Indeed, FAST provides a precise numerical model of FWT that makes it possible to get accurate numerical simulations with time-saving, low cost and easy for control implementation. The numerical based simulation is widely used in FWT researches (see General introduction). Nevertheless, it is still necessary to make experiments in a controlled and repeatable environment before its using control solutions in practical applications (scale 1).

In this chapter, experiments are made on a reduced scaled model of spar-buoy floating wind turbine, on which different controllers are applied. The main contributions of this chapter are therefore

- description of the experimental set-up;
- application of the controllers to the experimental set-up;
- performance comparison and analysis for a set of tuning parameters in specific scenarios.

5.2 Experimental set-up

Comparing with the traditional on-shore wind turbine, the design of an experimental set-up of floating one is much more complex due to the coupling between the hydrodynamics of the platform and the aerodynamics of the rotor. This coupling problem presents several challenges for FWT experimental set-up.

- first-of-all, the scaling issue between hydrodynamic phenomena and aerodynamic phenomena is regarded as the most important one. Different scale schemes should be used for the aerodynamics of rotor and the hydrodynamics of floater. However, these scale schemes cannot be simultaneously used for the FWT experimental set-up since they introduce difficulty in reproducing the coupling between aero-hydro dynamic forces (Jamieson and Hassan 2011; Martin et al. 2012; Bayati et al. 2017);
- then, with the increasing size of the turbines rotor, due to the constraints on the rotor of wind tunnel tests, it is not acceptable to model the rotor with a limited scale ratio.

Hence, in order to deal with the modeling difficulties caused by the coupling aerodynamic forces and hydrodynamic forces, real-time hybrid modeling approach (Arnal 2020; P. Chen, J. Chen, and Hu 2020; Urbán and Guancho 2019) is adopted.

5.2.1 Real-time hybrid method

The hybrid methodology (Carrion and Spencer Jr 2007) reproduces the behaviour of large-scale structure through numerical simulation and physical experiment simultaneously, and has been applied to the FWT system in recent years (Hall and A. J. Goupee 2018; Hall, A. Goupee, and J. Jonkman 2018; Vittori et al. 2018; Arnal 2020). In this work, the experiments are carried out in a wave tank. Then, the hybrid model is composed by a scaled floating structure and a numerical rotor model (modeled by FAST software). The whole system can be defined as a combination of basin experimental set-up and software-in-the-loop (SIL). While the experimental system is scaled in the wave tank, and its dynamics captured by sensors, the numerical model in SIL simulation is

used for the aerodynamic forces calculation in real-time. Then, the calculated aerodynamic forces are applied on the reduced scale system by an actuator¹. The illustrative drawing of this hybrid method is depicted Figure 5.1.

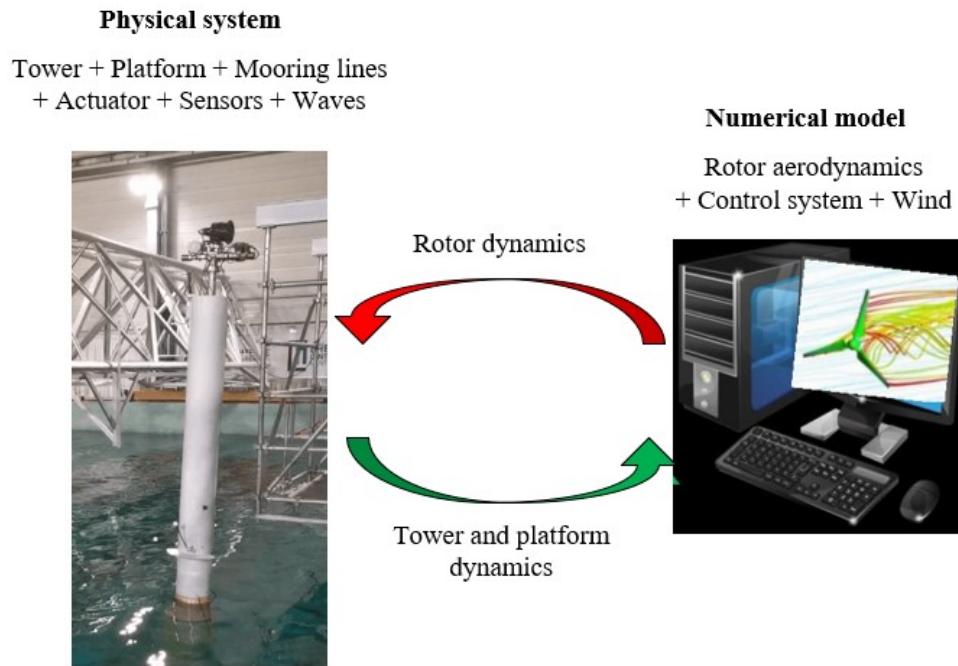


Figure 5.1 – The scheme of software-in-the-loop system, adapted from (Arnal 2020).

The whole experimental system consists of 3 parts

- the physical part in a wave tank, including the floating platform, the mooring lines, the tower, the different sensors and the actuator;
- the numerical part which is used for the calculation of aerodynamics and internal loads acting on the rotor in real-time;
- the real-time data acquisition system and control environment, collecting the measured signals from the physical part, controlling the actuator through the numerical part. It acts as a bridge between physical and numerical parts of data communication.

1. Notice that the actuator of the physical system is used to generate the aerodynamic forces calculated by the numerical model.

5.2.2 Reduced scale system

Experiments are made in the Ecole Centrale de Nantes (ECN) wave tank (see Figure 5.2). The wave tank experiments make it possible to test the response of the FWT hybrid system with different controllers under a repeatable environment. The physical system used in the experiments (Figure 5.2) is a 1/40 scale 10 MW spar floating wind turbine developed by (Arnal 2020) in the SOFTWIND project. This system is carried out for the purpose of developing innovative experimental test bench dedicated to the wave tank testing of floating wind turbines.

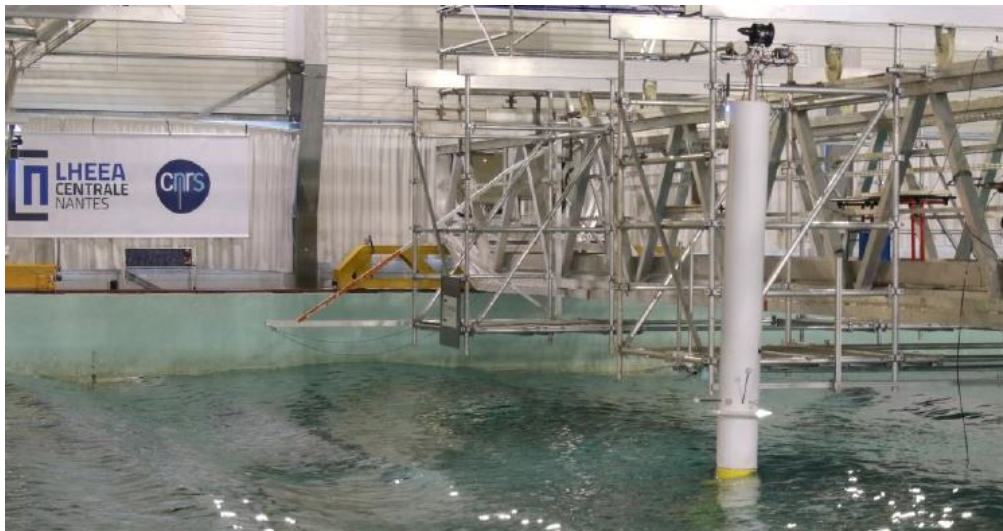


Figure 5.2 – Reduced scale floating wind turbine system in ECN wave tank (Arnal 2020).

The experimental system is scaled and based on the Technical University of Denmark (DTU) 10 MW onshore wind turbine (C. Bak et al. 2013) and the OC3 5 MW Hywind floating wind turbine (J. Jonkman 2010). The rotor nacelle assembly (RNA) and the tower are based on the full-scale DTU 10 MW wind turbine; the corresponding characteristics of the experimental model such as RNA mass, inertial, dimensions, ... are scaled. A spar-buoy floating structure is considered, and its main properties are based on the OC3 5 MW Hywind floating wind turbine.

The description of the experimental set-up is displayed in Figure 5.3. The tower consists of a flexible mast that is surrounded by an external casing. This casing is rigidly connected to the floater. Three mooring lines are connected between the floater and the bottom of the wave tank in order to limit the motions of the floater. At the top of the model is the RNA that is composed by the actuator and sensors, and the WIFI system that interacting with the real-time numerical model. As recalled in Footnote 1, the actuator allows to generate the aerodynamic forces calculated by the numerical simulations. The main properties of the experimental set-up, the target FWT and the estimated

uncertainties for each features are given in Table 5.1. More detailed descriptions can be found in (Arnal 2020).

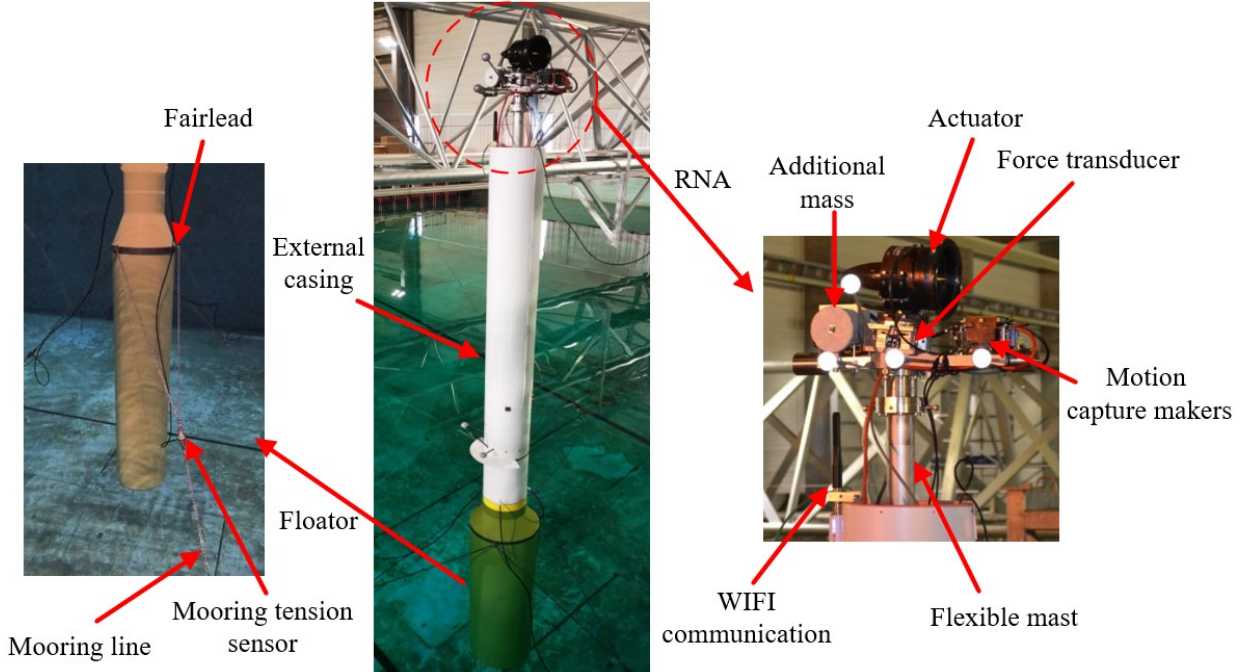


Figure 5.3 – Description of the FWT experimental set-up (Arnal 2020).

5.2.3 Numerical model

While the dynamics of tower, floater and mooring lines are scaled in the wave tank, the aerodynamics are computed numerically and reproduced thanks to the actuator. Considering the numerical computation, it is carried out in real-time by FAST software (see in Chapter 1).

5.3 Controller design

Recall once again that the control objectives of FWT in Region III are to regulate the power at its rated value meanwhile reducing the platform pitch motion. For all the controllers considered in the sequel, constant torque strategy is used, *i.e.* the generator torque Γ_g is fixed at its rated value Γ_{g0} , the power P regulation being regarded through the rotor speed Ω_r regulation according to

$$P = n_g \Gamma_{g0} \Omega_r. \quad (5.1)$$

2*Descriptions	Values		Uncertainties	
	Scale 1:40	Scale 1:1	Scale 1:40	Scale 1:1
RNA mass [kg]	12.45	7.97E+05	0.15	9.6E+03
Hub height above SWL [m]	3.03	121.2	0.01	0.4
Tower height [m]	2.666	106.6	0.005	0.2
Tower mass [kg]	13.48	8.63E+05	0.05	3E+03
Floater mass [kg]	303.8	1.94E+07	0.1	6.4E+03
Anchor depth [m]	5	200	0.01	0.4
Mooring line diameter [mm]	3.7	148	0.05	2
Fairleads depth [m]	-0.335	-13.4	0.005	0.2

Table 5.1 – Main properties of the experimental set-up (Arnal 2020).

Therefore, the control objectives are:

- regulation of the rotor speed Ω_r to its rated value Ω_{r0} ;
- reduction of the platform pitch motion, *i.e.* forcing the platform pitch rate to zero.

Three controllers will be implemented on the basin experiments:

- a GSPI controller based on the basic DTU (Hansen and Henriksen 2013) approach with re-tuned controller gains;
- a linear–quadratic regulator (LQR) developed by D-ICE company;
- the SAST controller proposed in Chapter 2.

A brief introduction of the GSPI and LQR control as well as some recalls of SAST control are given in the following subsections.

5.3.1 GSPI control

The reduced scale system in the wave tank is based on the DTU 10 MW wind turbine that is installed on a spar-buoy floating platform. In Region III, the DTU Wind Energy controller (Hansen and Henriksen 2013) is selected and applied. This controller is similar as the 5 MW reference wind turbine controller (J. Jonkman, Butterfield, et al. 2009), in which PI control and gain scheduling approaches are combined in order to regulate the power at its rated value. The collective blade pitch control β_{col} is obtained from the generator speed error $e(t)$ with proper tuned controller gains K_p

and K_i and reads as

$$\beta_{col} = K_p e(t) + K_i \int_0^t e(\tau) d\tau \quad (5.2)$$

with $e(t)$ defined as (with Ω_g the generator speed, and its rated value Ω_{g0})²

$$e(t) = \Omega_g - \Omega_{g0} \quad (5.3)$$

Notice that the control gain setting of the DTU 10 MW controller is efficient for an onshore wind turbines. Those gains have to be re-tuned to avoid negative damping excited by the floating platform. In fact, the onshore gain setting has been tested on the set-up, resulting in a large platform pitch motion and forcing to stop the test (Arnal 2020). Therefore, for the experimental set-up, controller gains tuned for the FWT are considered; a set of gains developed by Olav Olsen 10 MW FWT (Oo-Star) (Yu et al. 2018) is used so as to reduce the platform pitch motion. Furthermore, since the platform pitch natural frequency of Oo-star and the experimental spar-buoy floater are close, the controller gains selection are reasonable.

5.3.2 LQR control

A LQR controller implemented by D-ICE company is tested. Such optimal controller is based on the linear control methodology and has been already applied to the FWT (Hazim Namik, Karl Stol, and J. a. Jonkman 2008; Lemmer, Schlipf, and Cheng 2016). As detailed in Chapter 1, consider the 2 DOFs perturbed state-space linear model around the operating point (x_{op}, u_{op})

$$\dot{x} = A_{Avg} \cdot x + B_{Avg} \cdot u \quad (5.4)$$

with state vector $x = [\varphi \ \dot{\varphi} \ \Omega_r]^T$. $\Delta\varphi$, $\dot{\varphi}$ and Ω_r are the platform pitch angle variation, the platform pitch velocity variation and the rotor speed variation around the values at operating point (denoted by the subscript *op*) respectively. The operating point for rotor speed correspond to a rated rotor speed ($\Omega_{op} = \Omega_{r0}$) whereas the operating point for platform pitch velocity is equal to 0. The control input u of the system is the variation of the blade pitch angle with respect to β_{op} , its value at the operating point. Since all the states can be obtained in experiments, considering the following state feedback control law

$$u = -k_{LQR} \cdot x \quad (5.5)$$

with k_{LQR} the optimal control gain matrix. For the LQR controller, k_{LQR} is calculated such that the quadratic cost function J

$$J = \lim_{t \rightarrow \infty} \int_0^t [x^T Q x + u^T R u] dt \quad (5.6)$$

2. Recall that $\Omega_g = n_g \Omega_r$ and $\Omega_{g0} = n_g \Omega_{r0}$. As a consequence, this controller also regulates the rotor speed.

is minimized with Q and R the weighting matrices on the state vector x and input u respectively.

Once the controller gain k_{LQR} are optimally calculated, the control (5.5) forces the state vector x to the operating point. However, notice that the control (5.5) is carried out based on the linearized model that obtained around a single operating point, and such operating point depends on the wind speed and rotor speed (see Chapter 1). As a linear controller, the LQR control will lose its efficiency once the wind turbine is running away from the operating point. As a consequence, the controller gain k_{QR} need to be re-tuned under different wind speeds in order to keep high performances. Namely, in Region III, the LQR control reads as

$$u(t) = -k_{LQR}(t) \cdot x(t) \quad (5.7)$$

with $k_{LQR}(t)$ varying with the wind speed. As far as authors' knowledge, hundreds of controller gains have been tuned by D-ICE company in order to have targeted performances.

5.3.3 SAST control

In order to evaluate the performances of adaptive high order sliding mode algorithms on the experimental set-up, the simplified version of adaptive super-twisting (SAST) control displayed in Chapter 2 is selected; the main reason of this choice is that this control law is much easier for implementation. Notice that the adaptive super-twisting (ASTW) controller is also used in the experiment; however, the performances are not satisfied since the parameters are not well tuned, the results of ASTW being not shown in this work³.

Recalling Chapter 2, the rotor speed regulation and the platform pitch reduction are achieved by taking the advantage of the physical characteristics of the FWT, defining the desired rotor speed Ω_r^* as a function of platform pitch velocity $\dot{\varphi}$

$$\Omega_r^* = \Omega_{r0} - k\dot{\varphi} \quad (5.8)$$

Then, the control output y reads as

$$\begin{aligned} y &= \Omega - \Omega_r^* \\ &= \Omega_r - \Omega_{r0} + k\dot{\varphi} \end{aligned} \quad (5.9)$$

with k a positive constant. From (1.9)-(1.13), the relative degree of the output y with respect to

3. The current work had very limited time to test different controllers with different parameter tuning. Finally, no suitable ASTW parameters have been found.

β_{col} equals 1. Consequently, the sliding variable S is defined as

$$S = y \quad (5.10)$$

Therefore, according to the SAST algorithm detailed in Chapter 2, the control input reads as

$$\beta_{col} = -2L|S|^{\frac{1}{2}} \cdot \text{sign}(S) - \int_0^T \frac{L^2}{2} \cdot \text{sign}(S) dt \quad (5.11)$$

with L derived from the following dynamics ($L(0) > L_m$)

$$\dot{L} = \begin{cases} L(|S| - \mu), & \text{if } L > L_m \\ L_m, & \text{if } L \leq L_m \end{cases} \quad (5.12)$$

with μ the accuracy and L_m a small positive value making the controller gains smoothly and slightly increasing.

5.4 Experimental results and analysis

Before making basin experiments, the full scale experimental FWT is modeled thanks to the FAST code, and the numerical simulations are validated on FAST/SIMULINK environment. Such simulations are made in order to find an appropriate parameters tuning for the basin experiments. Table 5.2 shows the features of the FWT model. The SAST is tuned as $\mu = 0.1$, $L_m = 0.0001$ and the parameter k in (5.9) is equal to 10.

Description	Value
Rated rotor speed Ω_{r0}	9.6 rpm
Cut-in, rated, cut-out wind speed	4 m/s, 11.4 m/s, 25 m/s
Gear box ratio n_g	50
Maximum blade pitch rate	$\pm 8^\circ/\text{s}$

Table 5.2 – Properties of the FAST FWT model.

All the controllers have been implemented by D-ICE engineering on an industrial PC.

In the following subsection, two scenarios of experiments are made under different wind and wave conditions

- **Scenario 1:** SAST controller is used. The purpose of this scenario of test is to ensure that the proposed SAST controller can be successfully applied to the experimental set-up. Thus, the experiments are made under very simple wind and wave conditions: step wind and still water;

- **Scenario 2:** GSPI, LQR and SAST controllers are used. All these controllers are applied on the set-up under stochastic wind and irregular wave in order to evaluate their control performances in "real" conditions.

Notice that, all the comments are made in the sequel on the results obtained with tuning parameters and specific scenarios. Conclusions can not be generalized to all the possible conditions.

5.4.1 Scenario 1. Step wind and still water conditions

Figure 5.4 shows of the wind speed profile used during the experiments: the wind speed varies within Region III from 12 m/s to 25 m/s .

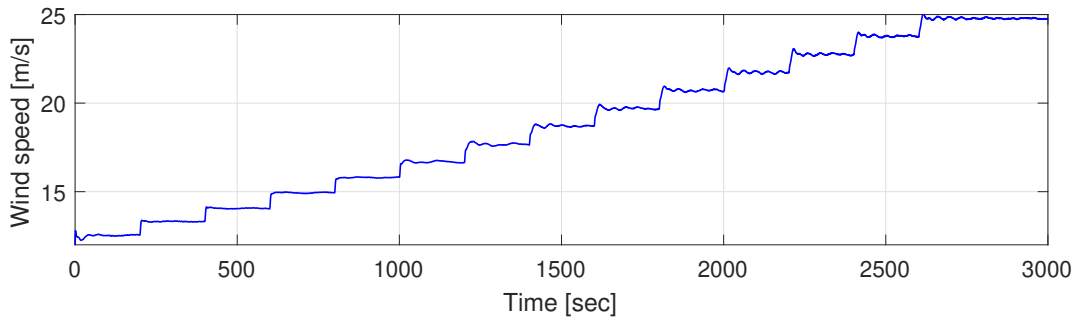


Figure 5.4 – **Scenario 1.** Wind profile (m/s) versus time (sec).

Figure 5.5 shows the evolution of rotor speed, platform pitch angle and its velocity and blade pitch angle. It is clear that the SAST controller allows to regulate the rotor speed at a value close to the rated one (9.6 rpm). The platform pitch rate is maintained around zero and has small variations, namely, the platform pitch motion is reduced. When the wind speed changes (Figure 5.4), some fluctuations in the rotor speed appears but after a transient time, the response of rotor speed converges close to the desired value. Moreover, since the platform pitch motion is limited, the platform pitch angle converges to a certain value at each wind speed with small fluctuations. In summary, under step wind condition and still water, the controller is able to achieve the control objectives among the whole Region III.

5.4.2 Scenario 2. Stochastic wind and irregular wave condition

In this scenario, the three controller, GSPI (DTU developed controller with FWT tuning), LQR (developed by D-ICE company) and SAST, are tested in the same stochastic wind and irregular wave conditions as shown in Figure 5.6. The wind and wave features are as following

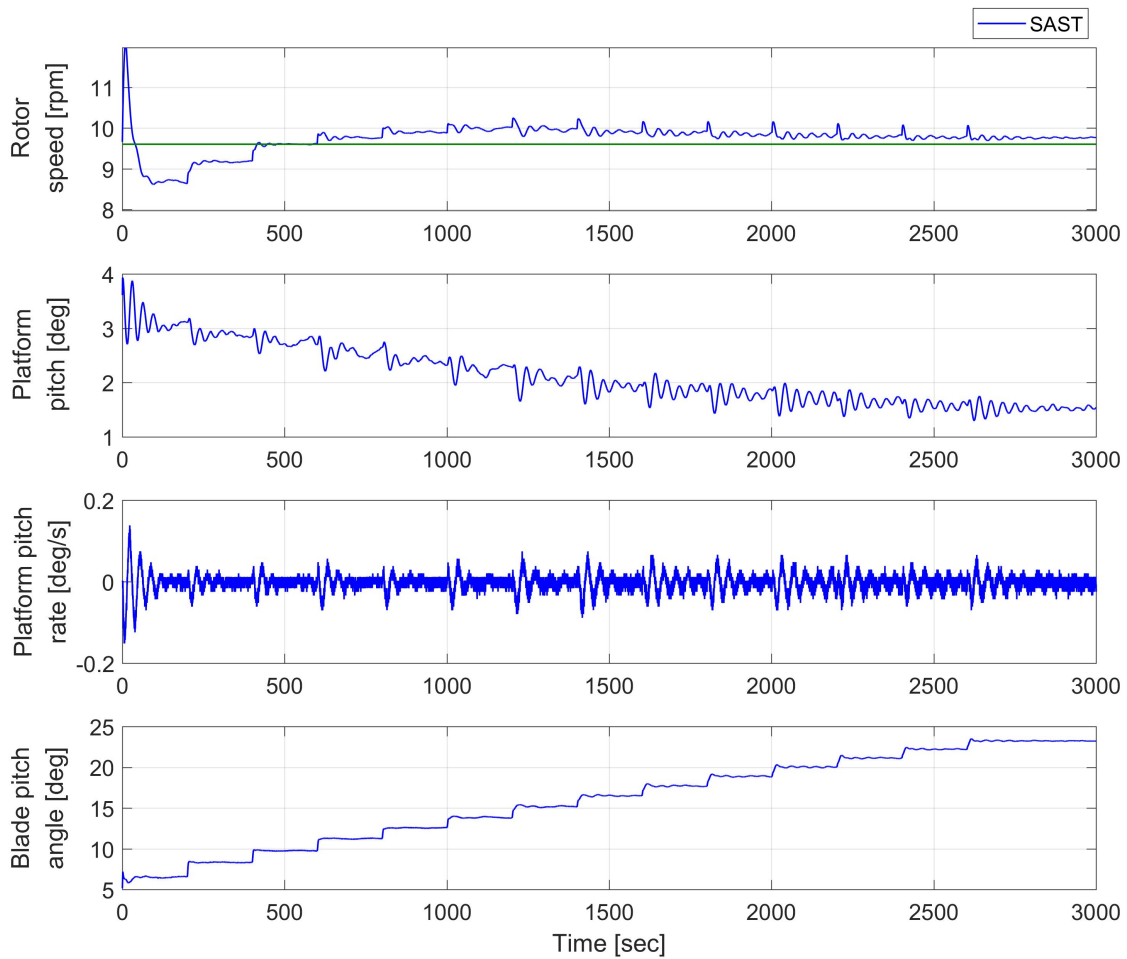


Figure 5.5 – **Scenario 1.** Measured variables of the FWT versus time (*sec*), obtained by SAST control. The green line in the first sub-figure indicates the rated rotor speed (*9.6 rpm*).

- 14m/s stochastic wind with 9% turbulence intensity;
- irregular wave with significant height of 3m, peak spectral period of 12s.

Recall that the tests have been made with a set of tuning parameters for each controller, and in some specific conditions.

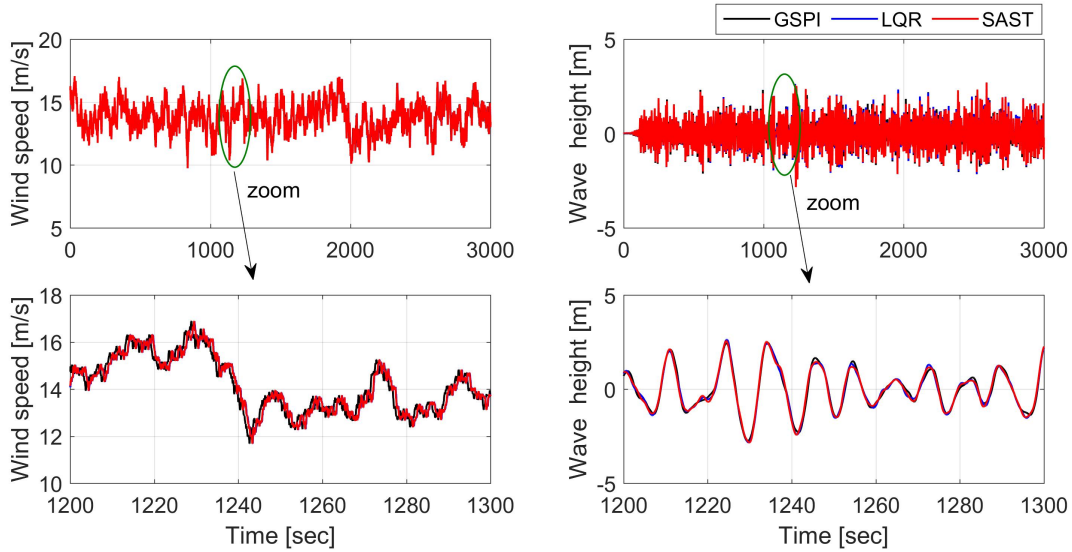


Figure 5.6 – **Scenario 2.** Wind speed (**left-m/s**) wave height (**right-m**) versus time (*sec*).

Figures 5.7 and 5.8 display rotor speed, blade pitch angle, platform motions and their rates for the three controllers. It is clear from these two figures that, firstly, the rotor speed responses obtained by LQR and SAST controllers have smaller fluctuations around the rated speed than the GSPI control. LQR and SAST controllers maintain the platform roll around a smaller value comparing with GSPI. For the platform roll and pitch angles, LQR and SAST controllers have smaller fluctuations than GSPI. Furthermore, they allow to get smaller roll and pitch rates. However, considering the blade pitch angle, the LQR control has much larger oscillations than the GSPI and SAST controllers⁴.

In order to have more precise and straightforward results comparison, the performances of the controllers are evaluated through the indicators

- root mean square (RMS) of rotor speed error from its rated value;

4. Notice that LQR controller has been tested by D-ICE in other conditions with other tuning parameters, and has allowed to get better results.

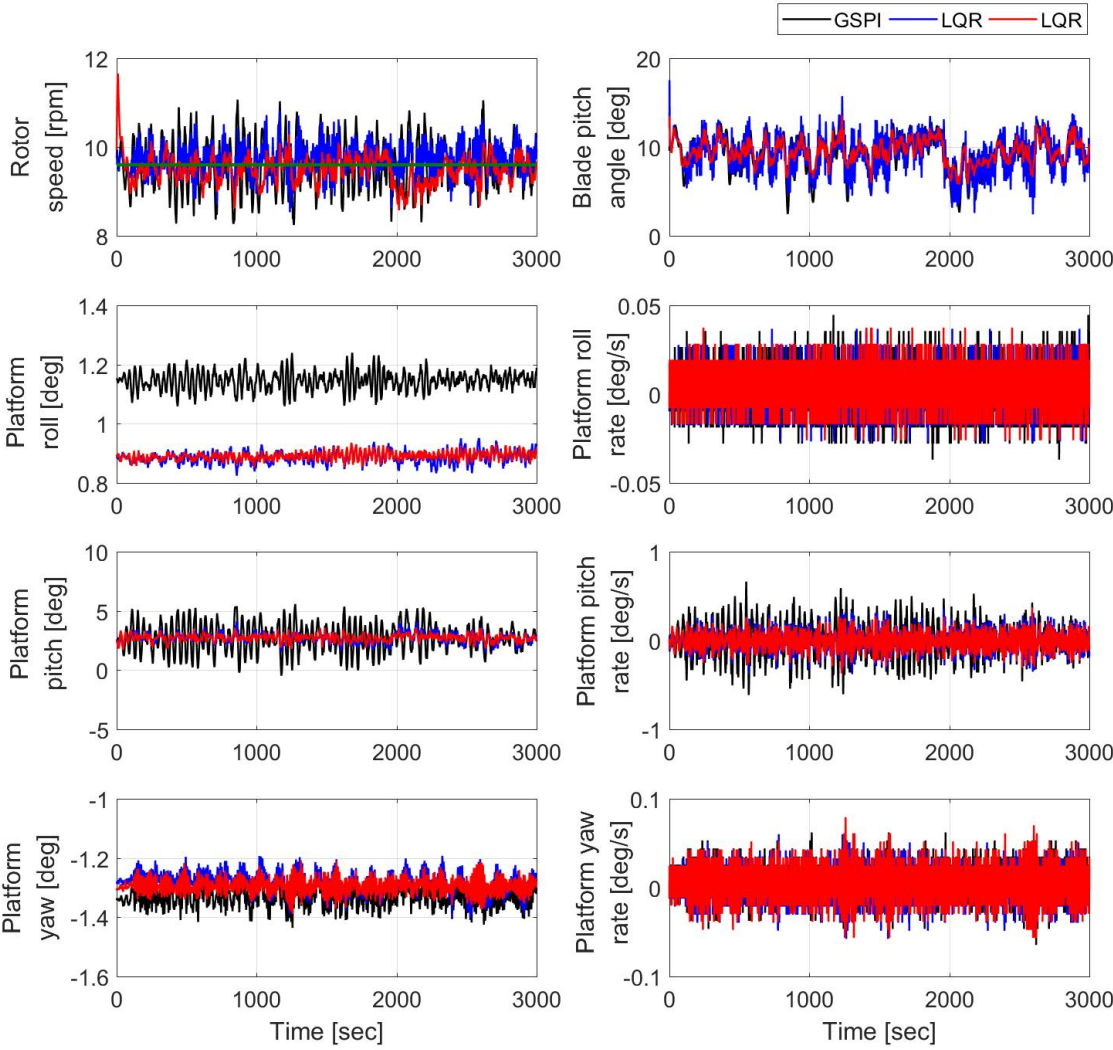


Figure 5.7 – **Scenario 2**. Measured variables of the experimental set-up versus time (*sec*), obtained by GSPI (black), LQR (blue) and SAST (red). The green line in the first sub-figure indicates the rated rotor speed (9.6 *rpm*).

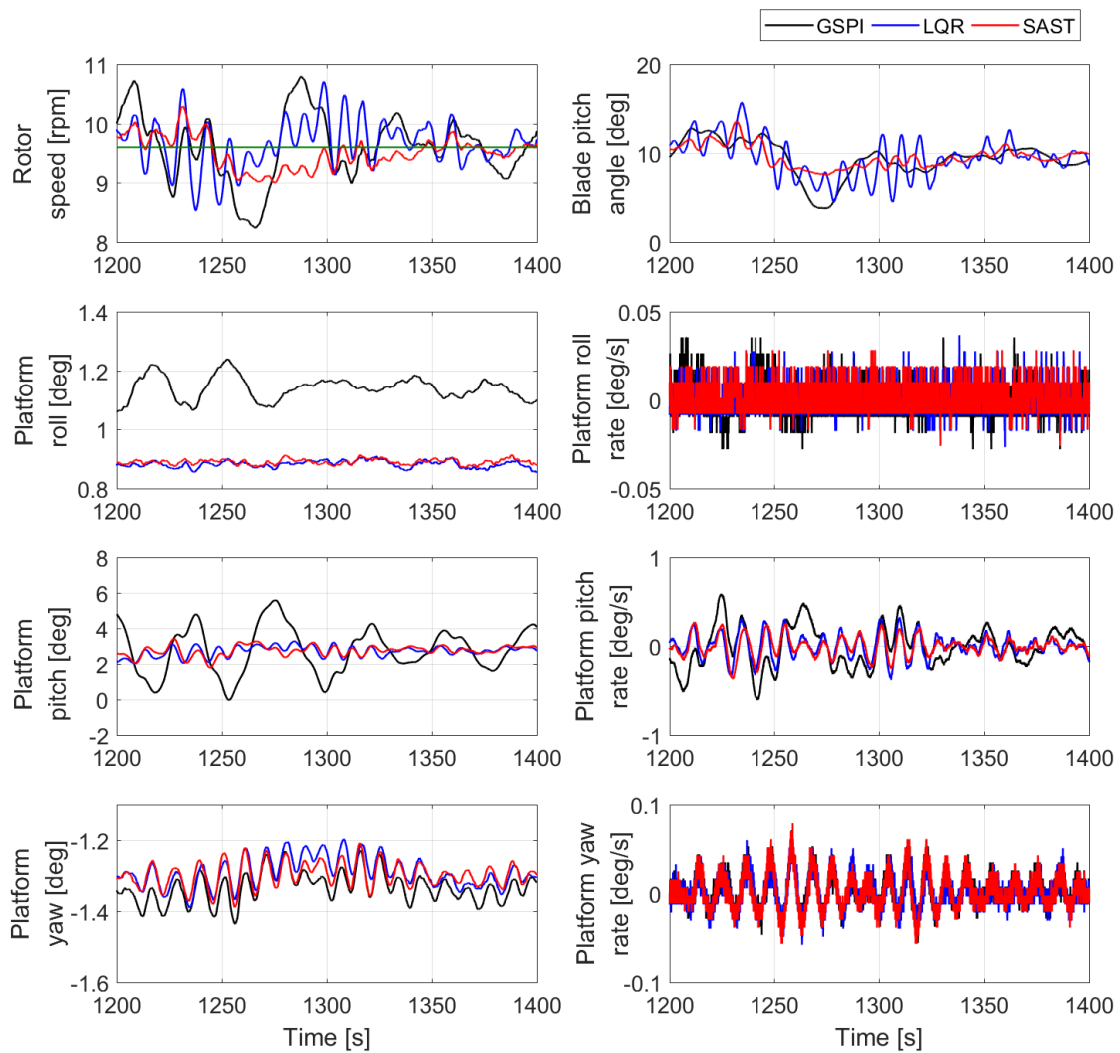


Figure 5.8 – **Scenario 2.** Zoom on measured variables of the experimental set-up displayed in Figure 5.7.

- RMS of platform motions and their rates;
- variation (VAR) of blade pitch angle.

All of those performance indicators are normalized with respect to the performances of GSPI control: the performance indicators of the GSPI controller are equal to 1. If the value of a normalized indicator is smaller than 1, it means the performance is better than GSPI; on the contrary, if the value of a normalized indicator is larger than 1, it means the performance is worse than GSPI. As shown in Figure 5.9, comparing with GSPI control, SAST and LQR strategies have better performances on the main control objectives: LQR control reduces the rotor speed error and platform pitch rate by 38% and 43% respectively versus GSPI, while the SAST control reduces rotor speed error by 37% and has a more platform pitch rate reduction, by 52%. For the rest of platform rotations and their rates, SAST and LQR controllers have similar performances. However, the variation of the blade pitch angle of LQR controller with the used tuning is much larger than SAST and GSPI controllers. It implies higher oscillations of the blade pitch angle and a higher request of the actuation system. Furthermore, notice that the controller gains of SAST can be adapted online whereas the LQR control needs large amount of parameters tuning around different operating points. Thus, SAST greatly reduces the tuning work load while getting globally the best performances of the three controllers.

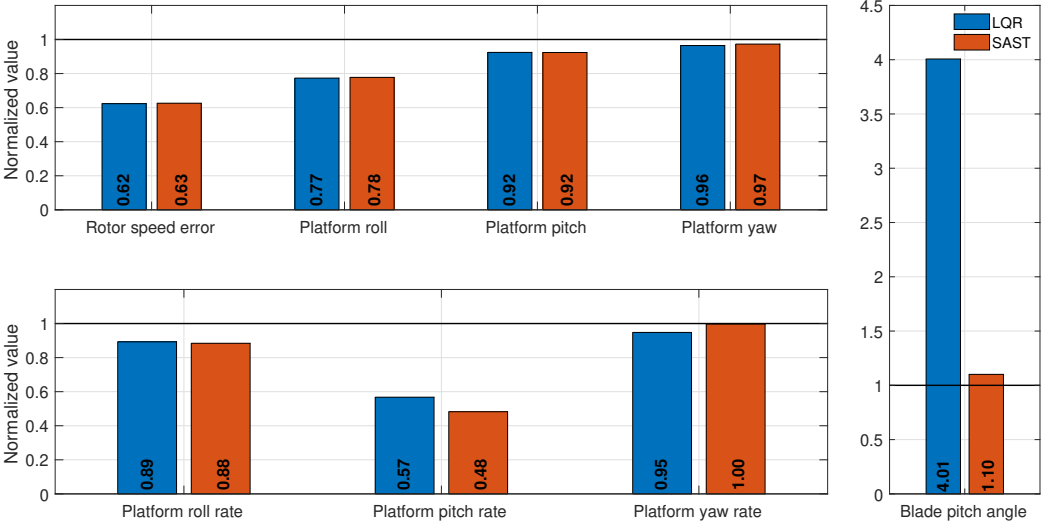


Figure 5.9 – **Scenario 2.** Normalized RMS (left)/VAR (right) values of performances indicators obtained by LQR (blue) and SAST (red) controllers.

Concerning fatigue load of the physical components of the experimental system, it is evaluated by

calculating the standard deviation (STD) of the tower base (TB) moments and the mooring line (ML) tensions. Such moments and tensions are measured by the sensors on the tower and on each of mooring lines. Similarly, the STD values are normalized versus GSPI as shown in Figure 5.10. SAST controller reduces the TB side-to-side and fore-aft loads by 12% and 6% respectively with respect to GSPI; for the TB moment load and the tensions of each mooring line, all the three controllers have similar performances.

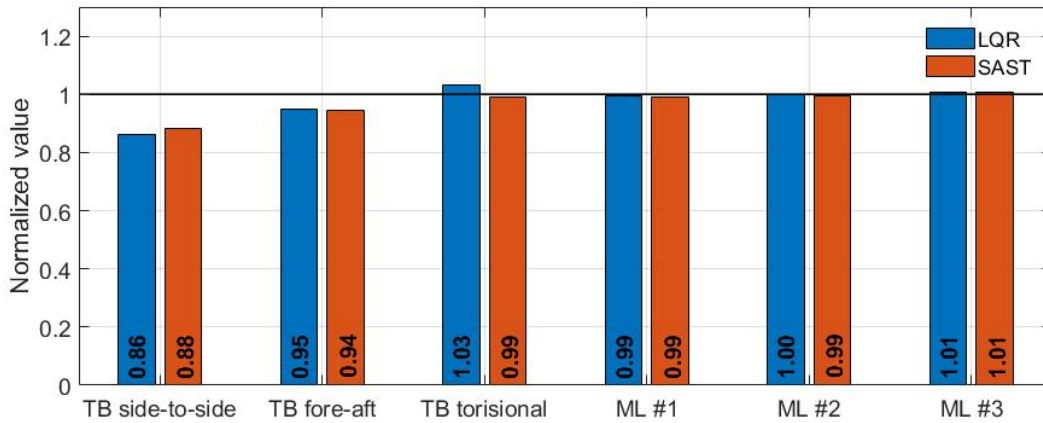


Figure 5.10 – **Scenario 2.** Normalized STD values of TB moments and ML tensions obtained by LQR (blue) and SAST (red) controllers.

Numerical replayed results

Recall that the rotor nacelle assembly is modeled by the FAST software and the aerodynamic forces are reproduced by the actuator. So, the moments of the blades cannot be physically measured. A numerical model of the experimental system has been built by FAST code. This numerical model is established at a full scale, from the measurements of the physical model. The experiments can be numerically replayed by FAST software. Such methodology provides a possibility to obtain the system variables that cannot be measured in the experiments as the blades moments. As detailed previously, the fatigue loads of the blade are crucial especially for the large scale FWT. The blade root (BR) moments of the three controllers are obtained by the FAST replayed simulations, as the damage equivalent loads (DEL).

Figure 5.11 displays the measured experimental data and the FAST replayed data. One can find that the FAST data is almost similar with the experimental data, expect a slight delay. By this way, FAST can accurately replay the experiments. To summarize, the numerical data can be used to evaluate the controller performances.

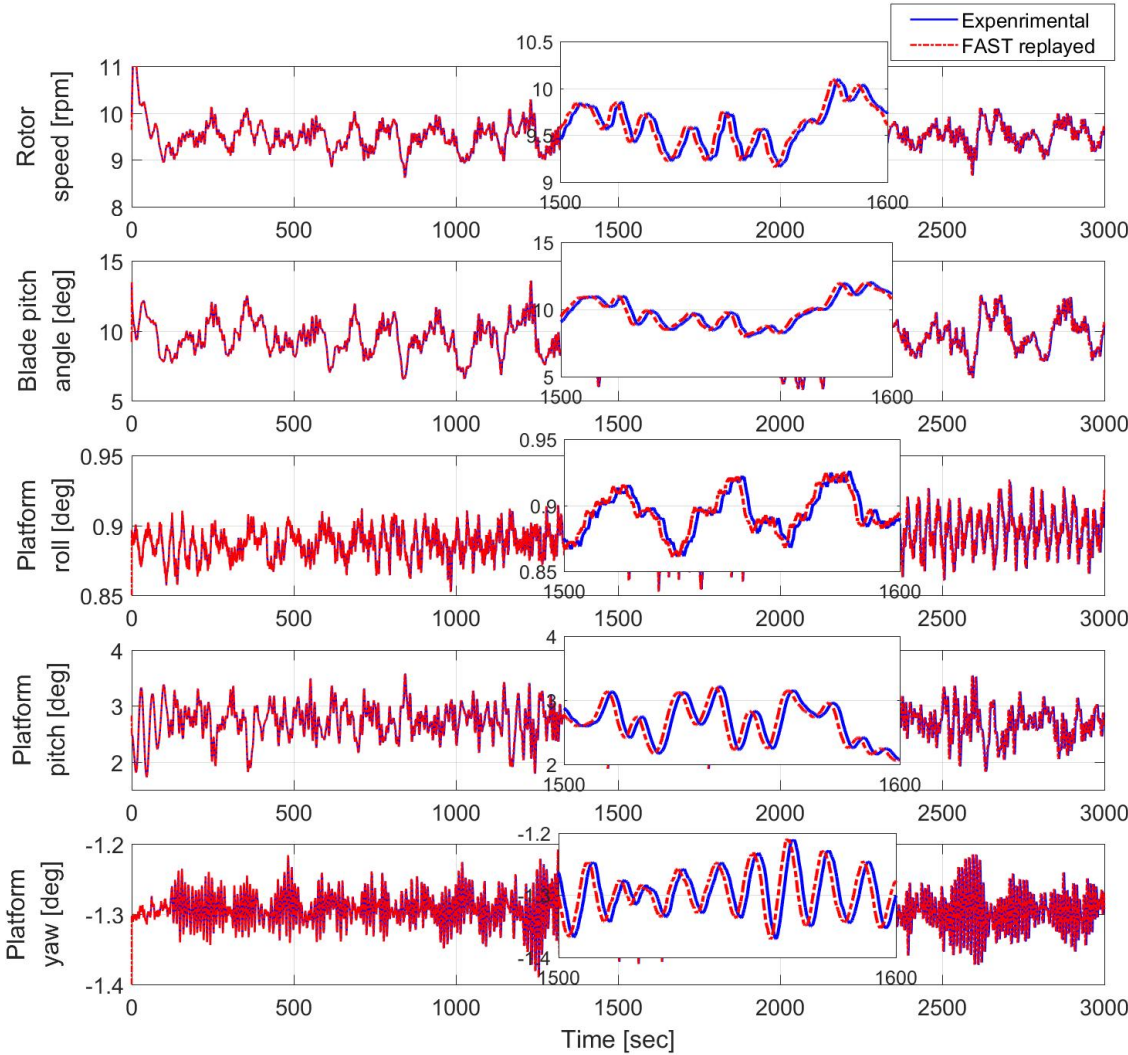


Figure 5.11 – **Scenario 2**. Measured experimental data (blue) and FAST replayed data (red) versus time (*sec*).

Figure 5.12 displayed the normalized DEL of BR moments obtained by the three controllers. Similarly, all the data are normalized such that, for GSPI controller, the quantity equals 1. Comparing with GSPI controller, SAST controller greatly reduces the DEL of BR flap-wise and pitch moments by 20% and 13% respectively whereas LQR tremendously increases those moments. Namely, SAST control could enlarge the lift-time of blades and thereby reduces maintenance cost and increases economic benefit.

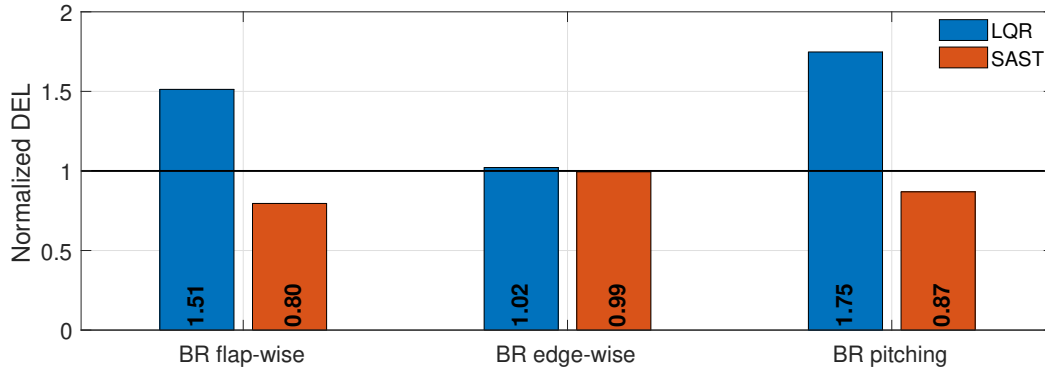


Figure 5.12 – **Scenario 2.** Normalized DEL values of BR loads obtained by LQR (blue) and SAST (red) controllers.

In summary, SAST and LQR controllers have greatly reduced the rotor speed error and platform pitch motion. However, the LQR control has high requirements for the blade pitch actuator. Concerning the fatigue load of the FWT components, the SAST control has best performances among the three controllers: it allows getting particularly much smaller DEL of blade root moments than LQR control. Moreover, such good performances of SAST are obtained thanks to a very reduced parameters tuning work load and system modeling information, making the implementation easier.

5.5 Conclusions

In this chapter, the proposed simplified adaptive super-twisting controller is applied to an experimental floating wind turbine set-up in the ECN wave tank. The experimental set-up has been designed by a hybrid method, and is composed by a reduced scale experimental set-up in the wave tank and a numerical one modeled by FAST. The SAST, LQR and GSPI controllers are briefly introduced and implemented on the scaled model.

Firstly, the SAST controller is checked under wind steps (among the whole Region III) and still water condition, that ensures the applicability of the controller. Then, all the three controllers are tested under stochastic wind and irregular wave conditions. Experimental results show that the

SAST controller greatly reduces the rotor speed error and platform pitch motion, allows to have small variations of blade pitch angle and structure fatigue loads. Given that the SAST controller needs a very reduced parameters tuning work load and system modeling information, it appears to be a very efficient and promising solution for the control of FWT.